Mobility Report for SEAKNOT-EU Project

Assessing Advanced Technology Cladding Materials in a Generic BWR Mark-I Reactor: Analysis of an SBO Scenario with the ASTEC Code

Eddy Gazzola

MSc in Nuclear Engineering

Mobility Details

- Sending Institution: University of Pisa, Prof. Sandro Paci
- Receiving Institution: KIT, Dr.-Ing. Fabrizio Gabrielli, Dr. Mauricio E. Cazado
- Mobility Period: 30th June 2025 – 19th December 2025

Report Overview

– Introduction and Scope

– Accident Scenario and Analysis Framework

– Results and Discussions

– Concluding Remarks and Lessons Learned

1 Introduction and Scope

This work focusses on the analysis of a Station Blackout (SBO) accident scenario in a generic BWR-4 Mark-I reactor (Peach Bottom Unit 2), by means of the ASTEC (Accident Source Term Evaluation Code), developed by ASNR, with the objective of assessing the impact of FeCrAl Advanced Technology Fuels (ATFs) alloys on severe accident progression, with a special focus on the in-vessel hydrogen production up to the cladding rupture. Since the Fukushima Daiichi accident in 2011, materials such as SiC, FeCrAl, and Cr-coated Zr alloys have gained increasing attention, partly because of their excellent oxidation resistance at high-temperature compared with Zircaloy, which is currently used.

In order to gain knowledge on the behaviour of ATF cladding materials alloys under representative high-temperature steam oxidation conditions, an intense experimental activity (Separate Effect Tests-SETs- and bundle tests) has been performed since years at the KIT QUENCH large test facility [1].

In parallel, in view of supporting the safety assessment of Nuclear Power Plants employing ATF cladding alloys, the capabilities of the integral codes, e.g., ASTEC, AC2, MELCOR, and MAAP, to consider such materials in their physical models are under evaluation.

A preliminary literature review was conducted to identify FeCrAl thermo-physical properties and oxidation correlations applicable to severe accident conditions. Based on this review, FeCrAl cladding was implemented in ASTEC by overriding the thermo-physical properties and oxidation correlation of the base Zircaloy model, since a dedicated FeCrAl model is not currently available in the code. As a consequence, the cladding is treated using the native Zr-based structure of the code, while the oxidation kinetics and material properties are overwritten with FeCrAl values through the input deck. Note that the information regarding the FeCrAl properties is based on the experimental outcomes from QUENCH SETs and the QUENCH-19 bundle test, performed in 2018 at KIT.

A series of simulations was then performed, followed by an Uncertainty and Sensitivity Analysis (UaSA) focused on the most influential parameters of the oxidation kinetics rate.
The analysis evaluates the impact of FeCrAl implementation on key safety-related figures of merit, with particular emphasis on hydrogen production up to the cladding failure.

This short report summarizes the main results and lessons learned from the SBO severe accident analysis, focusing on the engineering insights gained from the comparison between conventional Zircaloy and FeCrAl ATF cladding.

It is important to note that the ASTEC nodalization adopted for the generic BWR Mark-I reactor is identical for both the Zircaloy and FeCrAl cladding configurations. A detailed description of the nodalization can be found in the published work by O. Murat et al. (2024) [2].

2 Accident Scenario and Analysis Framework

A Station Blackout (SBO) scenario is considered, characterized by the loss of both off-site and on-site AC and DC power. Only limited DC power is assumed to be available to initiate and control the safety relief valves (SRVs) and the Automatic Depressurization System (ADS).
In addition, active safety systems are assumed to be unavailable in order to reduce scenario complexity, allow faster simulation runs, and enable a clearer interpretation of the results.

The analysis compares the behaviour of a conventional Zircaloy-based core with that of a core equipped with FeCrAl ATF cladding, highlighting differences in severe accident progression. The comparison mainly focuses on core heat-up, cladding degradation behaviour, and hydrogen production.

The following sections present the main results of the analysis, with emphasis on core degradation, hydrogen generation, and the key figures of merit used to assess the impact of ATF implementation under SBO conditions.

3 Results and Discussions

In this section, the main results of the early accident progression phase are presented for both Zircaloy and FeCrAl ATF cladding materials. The results are obtained from simulations performed with the ASTEC code for a Station Blackout (SBO) accident scenario, which was simulated up to the occurrence of basemat rupture.
Although late-phase accident phenomena, including corium formation and relocation, were considered in the simulations, the results presented in this report mainly focus on the early phase of the event. Particular attention is given to the impact on key thermo-hydraulic phenomena, as well as on cladding temperature evolution and hydrogen generation.
As core degradation progresses, the reliability of the results becomes increasingly limited due to the lack of experimental data and dedicated models describing the behavior of FeCrAl alloys after cladding failure, including interactions with the fuel and corium formation and relocation dynamics. Consequently, late-phase results are not reported and should be interpreted with caution. After the onset of the transient, a reactor SCRAM is assumed at t = 0 s, accom-

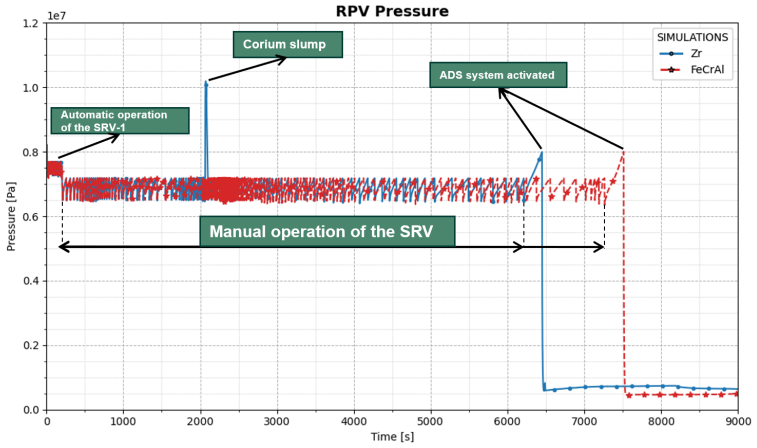

Figure 1: Pressure temporal variation inside the RPV.

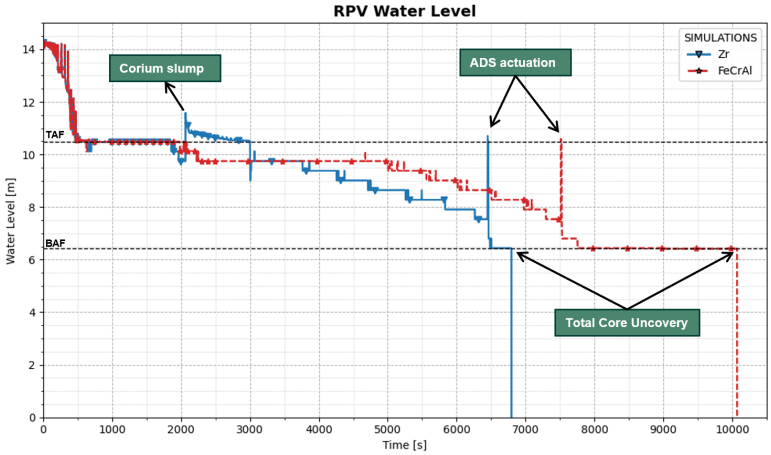

Figure 2: Avarage Water level temporal variation inside the RPV.

panied by the isolation of the main steam lines and feedwater lines. Figure 1 shows the time evolution of the reactor pressure vessel (RPV) pressure following the SCRAM. An automatic actuation of one safety relief valve (SRV) occurs shortly after the SCRAM and remains active for approximately 200 s. Subsequently, the manual operation of five SRVs is initiated in order to maintain the RPV pressure within the range of 64.9 – 71.8 bar. Manual SRV operation continues until the average water level in the core decreases to one-third of the Active Core Height. At this point, the Automatic Depressurization System (ADS) is actuated, leading to a rapid and significant pressure drop in the core region. For the two cladding materials analyzed, a delay of approximately 1000 s in the ADS actuation is observed for the FeCrAl cladding case compared to the Zircaloy reference. The delay in the core uncovery and the subsequent ADS system actuation for the two cladding materials can be seen also from the Figure 2, that shows the avaraged water level temporal variation inside the RPV for the two cladding materials.

As the accident scenario progresses and the coolant inventory is progressively lost from the reactor pressure vessel (RPV), a temperature escalation develops within the core. This behaviour is illustrated in Figure 3, which shows the time evolution of the Peak Cladding Temperature (PCT) for the different cladding MACROs (CLAD1, CLAD2, CLAD3, and CLAD4), which are defined within the radial meshes used to discretize the active core, from the innermost region (CLAD1) to the outermost one (CLAD4).
Each curve is reported up to the time at which the first cladding component becomes absent, marking the onset of significant cladding degradation for the corresponding MACRO.
Further details on the axial and radial discretization adopted for the active core, as well as on the overall nodalization of the reactor system, can be found in O. Murat et al. (2024) [2].

Following the initial temperature escalation, a temporary decrease in cladding temperature is observed, followed by a second temperature rise for both cladding materials. In the FeCrAl case, and particularly for the outermost cladding region (CLAD4), the first cladding component absence occurs much later than in the reference Zircaloy case.

The light purple dashed curve represents the PCT evolution of the CLAD4 MACRO for the Zircaloy case, assuming that the temperature trend is continued beyond the onset of the first cladding component absence. This curve is reported for comparison purposes only, in order to highlight the qualitative differences in the temperature evolution between the two cladding

materials. While the overall trend of this curve remains qualitatively similar to that observed for the FeCrAl cladding, the temperature escalation for Zircaloy starts earlier and proceeds more rapidly. The delayed onset of the second temperature escalation observed for the FeCrAl CLAD4 region can be explained by the slower reduction of the coolant inventory in the active core. As shown in the Figure 2, the progressive decrease of the water level is delayed in the FeCrAl ATF case, resulting in prolonged cooling of the core and, consequently, in a delayed heat-up of the corresponding cladding components.

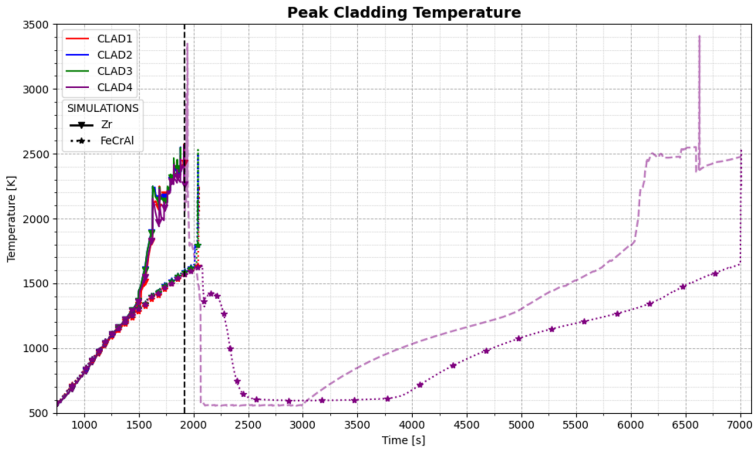

Figure 3: Peak Cladding Temperature (PCT) time evolution for the cladding MACROs defined within the radial meshes used to discretize the active core.

The cladding materials considered are the conventional Zircaloy and an FeCrAl ATF alloy, based on a generic B136Y3 composition (13 % Cr, 6 % Al, balance Fe). Thermo-physical and oxidation properties for the FeCrAl cladding were assessed from literature on alloys with equal or similar compositions.
In terms of oxidation reactions, Zircaloy and FeCrAl behave differently under high-temperature steam conditions: In the case of conventional Zircaloy cladding, high-temperature steam oxidation of zirconium is governed by the following exothermic reaction:

$$\mathrm{Zr} + 2\,\mathrm{H_2O} \longrightarrow \mathrm{ZrO_2} + 2\,\mathrm{H_2} \qquad \Delta H \approx -6\ \mathrm{MJ}/Kg_{Zr} \tag{1}$$

From reaction stoichiometry, the oxidation of 1 kg of zirconium leads to the production of approximately 44 g of hydrogen.
This reaction is characterized by a high reaction enthalpy and represents the main contributor to hydrogen generation during severe accident conditions in LWRs.

For FeCrAl-based ATF cladding, steam oxidation involves multiple alloying elements.
Iron, chromium, and aluminum can all react with steam, forming their respective oxides and releasing hydrogen [3].
In a general form, the oxidation of a metallic element M by steam can be expressed as:

$$2\,\mathrm{M} + 3\,\mathrm{H_2O} \longrightarrow \mathrm{M_2O_3} + 3\,\mathrm{H_2} \tag{2}$$

This generic formulation highlights the potential for hydrogen production associated with metal-steam reactions; however, in FeCrAl alloys the actual oxidation behavior strongly depends on

the specific element involved and on the prevailing oxidation regime.
In particular, iron oxidation represents the main source of hydrogen generation:

$$3\,\mathrm{Fe} + 4\,\mathrm{H_2O} \longrightarrow \mathrm{Fe_3O_4} + 4\,\mathrm{H_2} \qquad \Delta H \approx -0.90\ \mathrm{MJ}/kg_{Fe} \tag{3}$$

corresponding to approximately 48 g of hydrogen produced per kilogram of iron oxidized.
Aluminum oxidation, on the other hand, leads to the formation of a dense and protective alumina layer:

$$2\,\mathrm{Al} + 3\,\mathrm{H_2O} \longrightarrow \mathrm{Al_2O_3} + 3\,\mathrm{H_2} \qquad \Delta H \approx -17.6\ \mathrm{MJ}/kg_{Al} \tag{4}$$

Despite the potentially high hydrogen yield associated with iron and aluminum oxidation, the formation of a stable alumina scale significantly limits the overall oxidation rate of FeCrAl alloys. As a result, hydrogen production strongly depends on the temperature threshold governing the transition between alumina-controlled and iron-dominated oxidation kinetics.

Figure 4 shows the cumulative hydrogen mass produced by cladding oxidation (left axis), together with the average cladding temperature evolution (right axis).
A significant difference emerges between the ATF and the conventional Zircaloy cladding, both in terms of the total hydrogen mass generated and the onset of hydrogen escalation. For the FeCrAl cladding, the total hydrogen production remains below 300 kg, whereas for the Zircaloy case it exceeds 750 kg, corresponding to more than 150% higher hydrogen production for Zircaloy compared to the ATF cladding.
In addition, the FeCrAl case exhibits a delay of approximately 500 s in the onset of rapid hydrogen generation.
Another non-negligible aspect concerns the hydrogen production kinetics. Once oxidation is initiated, the FeCrAl cladding shows a steeper increase in the cumulative hydrogen curve, indicating a faster hydrogen generation rate with respect to Zircaloy. This behavior is consistent with the oxidation kinetics of iron-based oxides, while the overall hydrogen mass produced remains significantly lower.
The figure is truncated at 10000 s, as cladding oxidation is essentially completed beyond this time and the cumulative hydrogen mass remains constant.

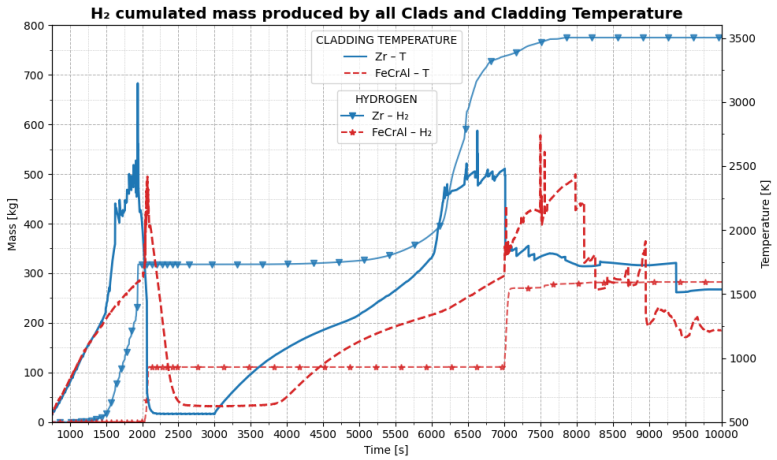

Figure 4: Total cumulated hydrogen mass produced by all the cladding components and avarage cladding temperature.

3.1 Uncertainty and Sensitivity Analysis

An Uncertainty and Sensitivity Analysis (UaSA) was performed to quantify the impact of selected model uncertainties on the main figures of merit of the SBO severe accident scenario. The analysis was carried out using the KATUSA (KArlsruhe Tool for Uncertainty and Sensitivity Analysis) tool, developed at KIT and coupled with the ASTEC code.

The objective of the Uncertainty and Sensitivity Analysis (UaSA) is to evaluate the impact of model uncertainties on the oxidation behavior of FeCrAl cladding under SBO conditions.
In particular, the analysis focuses on two uncertain parameters that are expected to have the strongest influence on the high-temperature steam oxidation kinetics of the FeCrAl alloy.

The first uncertain parameter is the pre-exponential factor A_{usa} appearing in the Arrhenius-type expression used to model the oxidation rate.

$$K_P = A_{usa} \exp\left(-\frac{E_a}{RT}\right) \tag{5}$$

The second parameter is the temperature threshold governing the transition between oxidation kinetics dominated by the formation of a protective alumina layer and those associated with iron-based oxide formation.
These two parameters were selected because they directly control both the onset and the intensity of the oxidation process, and therefore strongly affect hydrogen generation and heat release during severe accident progression.

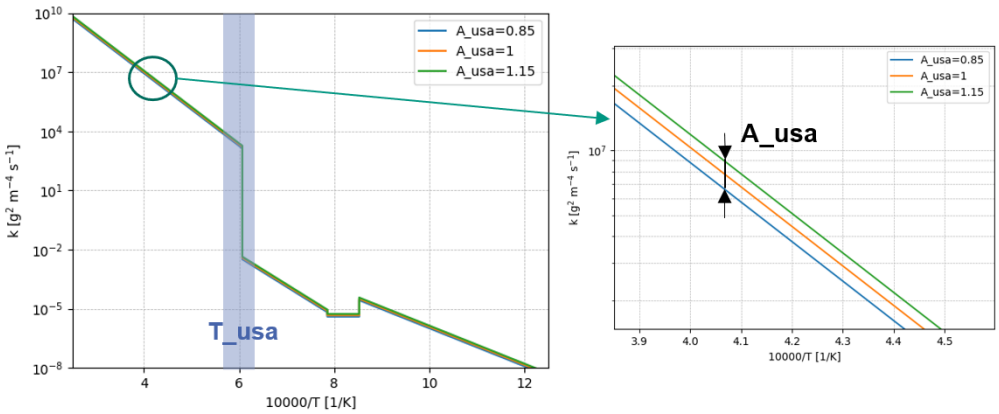

Figure 5: Uncertainty bands adopted for the Arrhenius pre-exponential factor and the switching temperature.

Figure 5 shows the uncertainty bands associated with A_{usa} and the switching temperature, derived from the analysis of available experimental results on FeCrAl oxidation. The bands were defined to encompass the different ranges of kinetic constants and transition temperatures observed for two distinct FeCrAl compositions tested in Separate Effect Tests at the KIT QUENCH facility, as reported by Kim et al. [5].

For both uncertain parameters, a uniform probability density function (PDF) was assumed, defined between a minimum and a maximum value. The selected uncertainty ranges, summarized in Table 1, were derived from the analysis of experimental oxidation data and are consistent with the uncertainty bands shown in Figure 5.
This choice reflects the limited availability of experimental data under severe accident conditions and avoids introducing additional assumptions on the statistical distribution of the parameters.

Table 1: Uncertainty ranges of the selected uncertain parameters used in the UaSA.

Uncertain Parameter	**Symbol**	**Min**	**Max**
Switching temperature	T_{switch}	-50 K	$+50$ K
Arrhenius pre-exponential factor	A_{gain}	0.85	1.15

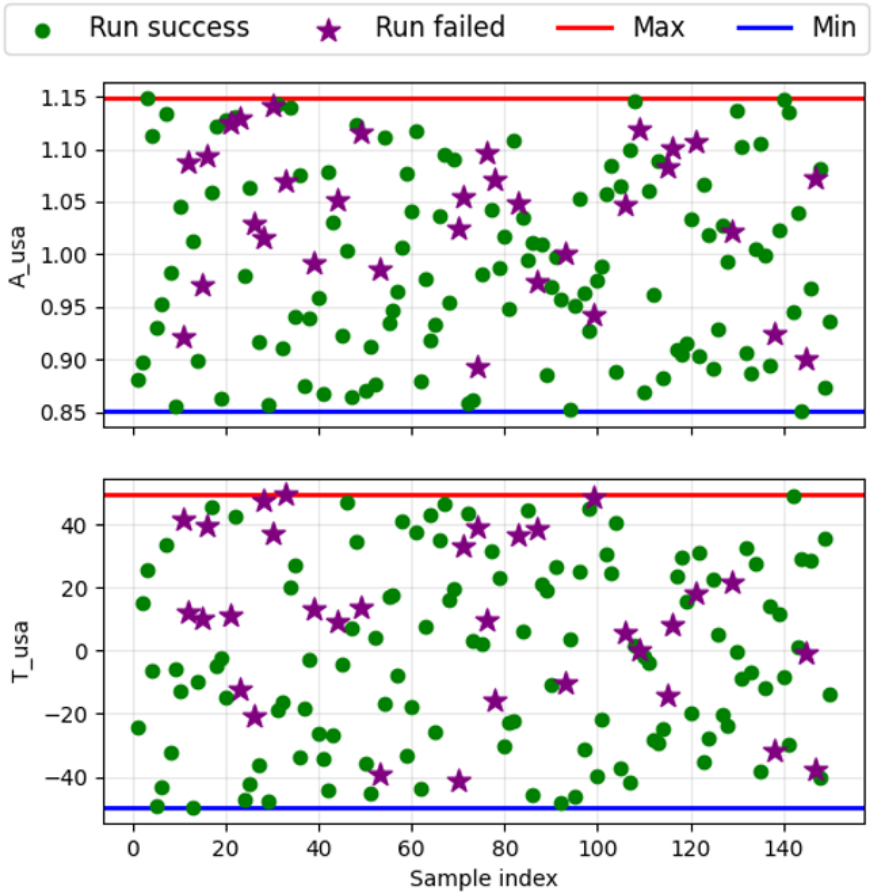

Figure 6: Uncertain Parameters (UPs) values for each sample.

Figure 6 shows the sampled values of the two uncertain parameters, a total of 150 simulations were performed within the selected uncertainty space and out of these, 32 runs did not complete successfully, the remaining simulations were used for the evaluation of the uncertainty bands and sensitivity trends of the selected figures of merit.

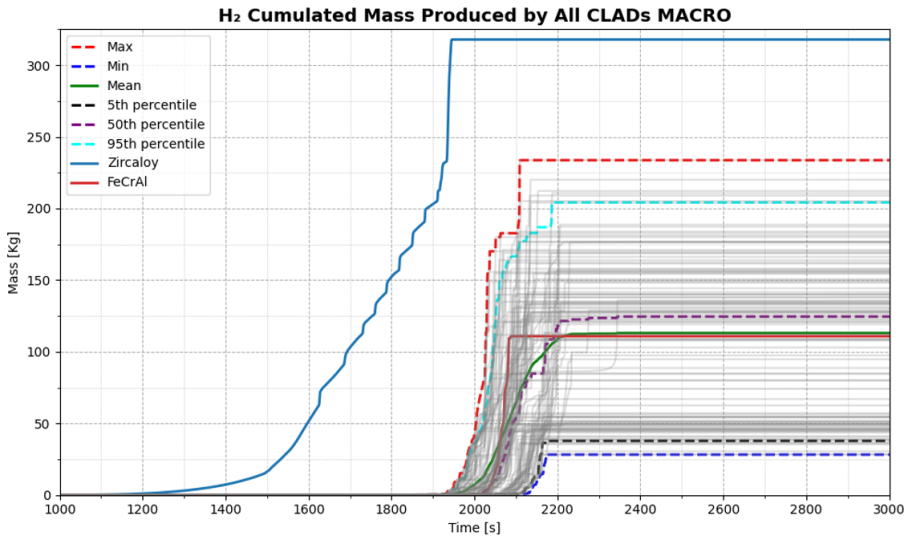

Figure 7: Cumulative hydrogen mass generated by all cladding components for the sampled realizations and the reference base cases.

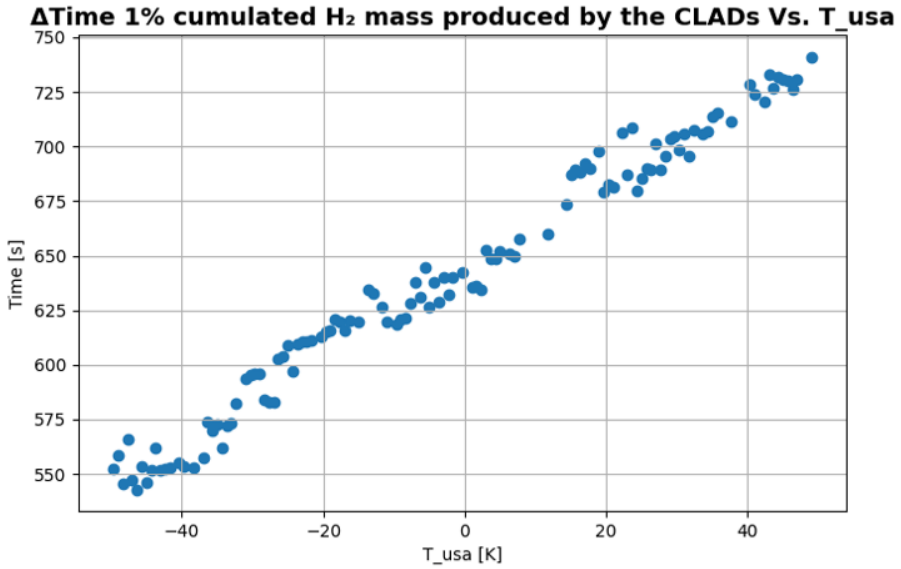

Figure 8: Time difference between the reference Zircaloy case and the sampled realizations to reach 1% of the total hydrogen mass produced by Zircaloy cladding.

The first figure of merit, shown in Figure 7, reports the cumulative hydrogen mass produced by all cladding components for the different FeCrAl samples, together with the reference curve corresponding to the Zircaloy case. A wide dispersion in hydrogen production is observed among the samples.
The uncertainty band spans from approximately 25 kg to about 225 kg, while the best-estimate FeCrAl case closely follows the mean value of the sampled distribution. The uncertain parameter exerting the strongest influence on the total hydrogen mass produced is the switching temperature in the oxidation correlation.

Figure 8 shows the time difference between the Zircaloy reference case and all FeCrAl samples required to reach 1% of the hydrogen mass produced by Zircaloy cladding (≈ 8 Kg).

A clear correlation with the switching temperature is observed: increasing the switching temperature leads to a larger delay in the onset of hydrogen production. This confirms that the switching temperature in the oxidation model is the dominant uncertainty parameter affecting hydrogen generation for FeCrAl cladding under SBO conditions.

4 Concluding Remarks and Lessons Learned

The analysis confirms that, under SBO conditions in a BWR-4 Mark-I reactor, the use of conventional Zircaloy cladding leads to rapid oxidation and significant hydrogen generation. The implementation of FeCrAl ATF cladding in ASTEC results in a markedly reduced oxidation rate and a substantial decrease in hydrogen production, with a delayed onset of hydrogen escalation. Note that based on the current knowledge on FeCrAl alloys and on the absence of dedicated physical models in integral codes for predicting the behaviour of highly degraded cores loaded with the FaCrAl materials, results beyond the cladding rupture are highly questionable.
The Uncertainty and Sensitivity Analysis highlights the oxidation kinetics—specifically the switching temperature in the oxidation correlation—as the dominant parameter governing hydrogen generation.
Despite the presence of large uncertainty bands, these results underline the critical role of oxidation modeling in severe accident analysis and confirm that accurate representation of FeCrAl oxidation behavior is essential to reliably assess the potential benefits of ATF concepts under SBO conditions.

Bibliography

References

[1] Stuckert, J., Grosse, M., Steinbrück, M., & Terrani, K. (2022). *Results of the bundle test QUENCH-19 with FeCrAl claddings.* Institut für Angewandte Materialien, Angewandte Werkstoffphysik, Karlsruher Institut für Technologie: Karlsruhe, Germany.

[2] Murat, O., Sanchez-Espinoza, V., Gabrielli, F., Wang, S., Stieglitz, R., & Queral, C. (2024). *Improved analysis of the short-term station blackout accidents of the Peach bottom unit-2 reactor with ASTEC including radiological impact and statistical analysis with JRODOS.* Nuclear Engineering and Design, 420, 113012.

[3] Steinbrueck, M., Grosse, M., Tang, C., Stuckert, J., & Seifert, H. J. (2024). *An overview of mechanisms of the degradation of promising ATF cladding materials during oxidation at high temperatures.* High Temperature Corrosion of Materials, 101(4), 621-647.

[4] Mauricio E. Cazado, Zaira I. Jiménez-Balbuena, Fabrizio Gabrielli, Victor H. Sánchez-Espinoza. *Impact of Advanced Technology Fuel Cladding Materials on the Progression of Severe Accidents in a Generic Natural-Circulation iPWR.*

[5] Kim, C., Tang, C., Grosse, M., Maeng, Y., Jang, C., & Steinbrueck, M. (2022). *Oxidation mechanism and kinetics of nuclear-grade FeCrAl alloys in the temperature range of 500–1500 C in steam.* Journal of Nuclear Materials, 564, 153696.